1 **Diverse mixing states of amine-containing single particles in Nanjing,**

2 **China**

3 Qi En Zhong[1,2], Chunlei Cheng[1,2]*, Zaihua Wang[3]*, Lei Li[1,2], Mei Li[1,2], Dafeng Ge[4,5],

4 Lei Wang[4,5], Yuanyuan Li[4,5], Wei Nie[4,5], Xuguang Chi[4,5], Aijun Ding[4,5], Suxia

5 Yang[2,6], Duohong Chen[7], Zhen Zhou[1,2]

7 [1]Institute of Mass Spectrometry and Atmospheric Environment, Guangdong

8 Provincial Engineering Research Center for on-line source apportionment system of

9 air pollution, Jinan University, Guangzhou 510632, China

10 [2]Guangdong-Hongkong-Macau Joint Laboratory of Collaborative Innovation for

11 Environmental Quality, Guangzhou 510632, China

12 [3]Institute of Resources Utilization and Rare Earth Development, Guangdong

13 Academy of Sciences, Guangzhou 510651, China

14 [4]Joint International Research Laboratory of Atmospheric and Earth System Sciences

15 (JirLATEST), School of Atmospheric Sciences, Nanjing University, Nanjing 210023,

16 China

17 [5]Collaborative Innovation Center of Climate Change, Jiangsu Province, Nanjing

18 210023, China

19 [6]Institute for Environment and Climate Research, Jinan University, Guangzhou

20 510632, China

21 [7]State Environmental Protection Key Laboratory of Regional Air Quality Monitoring,

22 Guangdong Environmental Monitoring Center, Guangzhou 510308, China

24 *Correspondence to: Chunlei Cheng (chengcl@jnu.edu.cn) and Zaihua Wang (zaihuawang@163.com)

25 Tel: 86-20-85225991, Fax: 86-20-85225991

27
28
29

Abstract: The mixing states of particulate amines with different chemical components are of great significance in studying the formation and evolution processes of amine-containing particles. In this work, the mixing states of single particles containing trimethylamine (TMA) and diethylamine (DEA) are investigated using a high-performance single-particle aerosol mass spectrometer located in Nanjing, China, in September 2019. TMA- and DEA-containing particles accounted for 22.8% and 5.5% of the total detected single particles, respectively. The particle count and abundance of the TMA-containing particles in total particles notably increased with enhancement of ambient relative humidity (RH), while the DEA-containing particles showed no increase under a high RH. This result suggested the important role of RH in the formation of particulate TMA. Significant enrichments of secondary organic species, including $^{43}C_2H_3O^+$, $^{26}CN^-$, $^{42}CNO^-$, $^{73}C_3H_5O_2^-$, and $^{89}HC_2O_4^-$, were found in DEA-containing particles, indicating that DEA-containing particles were closely associated with the aging of secondary organics. The differential mass spectra of the DEA-containing particles showed much higher abundance of nitrate and organic nitrogen species during the nighttime than during the daytime, which suggested that the nighttime production of particulate DEA might be associated with reactions of gaseous DEA with HNO_3 and/or particulate nitrate. In the daytime the decrease of DEA-containing particles was observed with the enrichment of oxalate and glyoxylate, which suggested a substantial impact of photochemistry on the aging process of DEA-containing particles. Furthermore, greater than 80% of TMA- and DEA-containing particles internally mixed with nitrate, while the abundance of sulfate was higher in the DEA-containing particles (79.3%) than in the TMA-containing particles (55.3%). This suggested that particulate DEA existed both as nitrate and sulfate aminium salts, while the particulate TMA primarily presented as nitrate aminium salt. The different mixing states of the TMA- and DEA-containing particles suggested their different formation processes and various influencing factors, which are difficult to be investigated using bulk analysis. These results provide insights into the discriminated fates of organics during the evolution

60 process in aerosols, which helps to illustrate the behavior of secondary organic

61 aerosols.

62 **Keywords:** Amines; Single particle; Mixing state; Nighttime chemistry; Aminium

63 salts.

64

65 1 Introduction

66   Amines are ubiquitous organic components in aerosols and have a wide range of

67 sources, including animal husbandry, industrial emissions, vehicle exhaust, biomass

68 burning, vegetation emissions, and ocean emissions (Ge et al., 2011b; Facchini et al.,

69 2008; Youn et al., 2015). Due to being highly water-soluble and having strong

70 alkaline properties, amines play an important role in new particle formation and

71 substantially contribute to the secondary organic aerosol (SOA) mass (Zhao et al.,

72 2011; Tao et al., 2016). The formation processes of particulate amines are commonly

73 associated with the gas-to-particle partitioning of gaseous amines and acid-base

74 reactions in the particles (Ge et al., 2011a; Pratt et al., 2009). Therefore, ambient

75 relative humidity (RH) (Rehbein et al., 2011; Zhang et al., 2012), temperature (Huang

76 et al., 2012), particle acidity (Pratt et al., 2009; Rehbein et al., 2011),

77 amine-ammonium exchange (Chan and Chan, 2013; Chu and Chan, 2017; Qiu et al.,

78 2011), and oxidants (Tang et al., 2013; Price et al., 2016) all influence the formation

79 of particulate amines.

80   Many field observations have been used to investigate the influence of RH on the

81 formation of amines. A high RH is beneficial for the formation of amines in most

82 cases. Zhang et al. (2012) observed a sharp increase in trimethylamine (TMA) during

83 fog events with high RH. Zhou et al. (2019) found that the concentrations of low

84 molecular weight (LMW) amines increased significantly under high RH conditions (>

85 90%). According to the seasonal distributions of amines during the summer and

86 winter, low temperature was found to be favorable for the partitioning of gaseous

87 amines into particles. Huang et al. (2012) found that the number fraction (N_f) of

88 amine-containing particles during winter was four times higher than that during

89 summer.

90   Gaseous amines can react with sulfuric acid, nitric acid, and organic acids to

91 form aminium salts, which underscores the important roles of sulfate and nitrate

92 information of particulate amines (Berndt et al., 2010; Murphy et al., 2007). Berndt et

93 al. (2010) and Wang et al. (2010) found that the formation of aminium salts via a

94 neutralization reaction can affect the growth of particles and the generation of SOAs.

95 Although the concentrations of amines are generally lower than ammonia, the

96 amine-ammonium exchange still contributes to particulate amine formation due to the

97 stronger alkalinity of amines compared to ammonium (Ge et al., 2011b; Sorooshian et

98 al., 2008). Chan et al. (2013) found that the exchange reactions between ammonia and

99 amines showed different reaction rates and product ratios with changes in the aerosol

100 phase state. Qiu et al. (2011) also found that amines can exchange with ammonium to

101 release ammonia. The particulate amines produced from the above pathways and

102 reactions constitute a substantial proportion of the SOAs that impact the physical and

103 chemical properties of fine particles. In addition to the direct contribution of the SOA

104 mass, the oxidation of amines by OH radicals, NO_3 radicals, and O_3 is also a

105 substantial source of SOA production (Price et al., 2016; Tong et al., 2020). Different

106 amines exhibit inconsistent behaviors under the same oxidation environments (NO_3

107 radicals, OH radicals, or ozone) (Price et al., 2014; Silva et al., 2008; Murphy et al.,

108 2007). In chamber studies, the oxidation of TMA and diethylamine (DEA) by OH vs.

109 NO_3 radicals resulted in different SOA yields, with differences greater than one order

110 of magnitude (Tang et al., 2013). Furthermore, even the same amine showed

111 completely different SOA yields due to OH and NO_3 radical oxidation. Also, the same

112 amine showed distinct trends under the different temperature changing trends. The

113 formation and oxidation processes of particulate amines are not well understood, and

114 these processes require additional comprehensive field observational studies in order

115 to be elucidated.

116   Most of the field observations did not distinguish between the different behaviors

117 of each type of amine molecule under the same ambient influencing factors. Actually,

118 due to the different mixing states of amines with other chemical components, the

119 amine molecules typically exhibited different behaviors in terms of being oxidized by

120 OH radicals, forming aminium salts, and altering the hygroscopicity of the particles

121 (Healy et al., 2015; Cheng et al., 2018; Chu et al., 2015; Price et al., 2016). Therefore,

122 the formation processes of the different amines are important to reveal the evolution

123 process of organic aerosols (OAs), and these processes are of great significance to

124 comprehensively understand the influencing factors of OA production.

125   The mixing states of organics in single particles are commonly investigated by

126 electron microscope and mass spectrometry (Yu et al., 2019; Li et al., 2016a; Cheng

127 et al., 2018). The technique of electron microscope coupled with energy dispersive

128 X-ray spectrometry (EDX) can provide the morphological, physical and some

129 chemical information of organics in single particles (Li et al., 2016b; Li et al., 2021).

130 However, electron microscope coupled with EDX cannot distinguish and identify the

131 specific organic molecules (Li et al., 2016b), which is incapable of analyzing amines

132 in single particles. The technique of single particle mass spectrometry can identify the

133 real-time presence and relative abundance of specific organic ions, which provides

134 substantial data to understand the sources, formation and evolution processes of

135 selective organic markers, providing a feasible approach to investigate the formation

136 processes of different particulate amines (Cheng et al., 2018; Chen et al., 2019;

137 Angelino et al., 2001). Chen et al. (2019) found that high RH was favorable for the

138 uptake of DEA, leading to a DEA-rich substance in the particle phase both during

139 winter and summer. However, Cheng et al. (2018) and Lian et al. (2020) found that

140 RH was not strongly correlated with the formation of amine-containing particles

141 during winter and summer. Pratt et al. (2009) reported that more acidic particles

142 during summer were favorable for the formation of aminium salts compared with the

143 particles present during autumn, indicating that the particle acidity affected the gas to

144 particle partitioning of amines. Rehbein et al. (2011) found more TMA entered the

145 particles as the amount of acidic particles increased. Based on these studies, although

146 the influences of ambient RH and particle acidity on the specific type amines formed

147 have been reported, yet comparative studies between different amines under the same

148 atmospheric environment using field observation are lacking.

149   In the present study, the mixing states of TMA- and DEA-containing single

150 particles are investigated during autumn using a high performance single particle

151 aerosol mass spectrometer (HP-SPAMS) located in Nanjing, China. Nanjing is a

152 typical megacity in the Yangtze River Delta (YRD), which is downwind of other

153 megacities including Shanghai, Changzhou, Suzhou, and Wuxi (Figure S1). In

154 addition, Nanjing suffers from heavy loadings of anthropogenic pollutants as well as

155 the complex impacts of biogenic and ship emissions (Xu et al., 2021; Zhao et al.,

156 2020; Ding et al., 2013a). The investigation of mixing states of amines in Nanjing

157 helps to explorer the formation and evolution processes of OAs. Two types of

158 amine-containing particles exhibited different mixing states with secondarily

159 produced OA species. The influences of ambient RH, T, and particle acidity on the

160 mixing states of the two amine-containing particles are evaluated. In addition, the

161 potential heterogeneous formation of DEA during the nighttime is also discussed. The

162 results revealed the distinct chemical behaviors of TMA- and DEA-containing

163 particles and implied the potential role of DEA as an indicator of the aging process of

164 OA.

165 **2 Experimental methods**

166 **2.1 Sampling site**

167   Ambient single particles were sampled using the HP-SPAMS from September 2–

168 16, 2019, in Nanjing, China. The campaign was conducted at the Station for

169 Observing Regional Processes of the Earth System (SORPES) station in Nanjing

170 University Xianlin Campus (Ding et al., 2016; Ding et al., 2013a; Ding et al., 2013b;

171 Liu et al., 2021). The instrument was set up on top of a small hill (40 m above the

172 ground) on the Nanjing University campus. The ambient single particles were

173 introduced into the HP-SPAMS through a copper tube.

174 **2.2 Instrumentation of the HP-SPAMS**

175   In this work HP-SPAMS (Hexin Analytical Instrument Co., Ltd., China) was

176   used to detect single particles. The design and principles of SPAMS had previously

177   been described in detail (Li et al., 2011). In short, particles are introduced into the

178   aerodynamic lens through a critical orifice at a flow rate of 75 mL/min (Gong et al.,

179   2021; Li et al., 2011). Individual particles are focused and accelerated to specific

180   velocities, which are detected by two continuous diode Nd:YAG laser beams (532 nm)

181   and then ionized using a pulsed Nd:YAG laser (266 nm). Finally, the z-shaped bipolar

182   time of the flight mass spectrometer is used to detect the generated ions. The

183   improvements and modifications from the SPAMS to the HP-SPAMS are

184   comparatively presented below. The improvement in the SPAMS primarily includes

185   three parts: the application of a concentration device, a delay extraction technology,

186   and a multichannel acquisition technology (Chen et al., 2020; Li et al., 2018). First,

187   the addition of the concentrator increases the injection flow rate by six times, which

188   allows for improved separation of gas and particles. Second, the generated ions from

189   the laser ionization of single particles firstly enter the zone without electric field. Then,

190   the pulsed electric field will be added to accelerate the same kind of ions flying to the

191   detector. This pulsed electric field instead of the constant electric field will prevent

192   the initial deflection of same kind of ions, and the pulsed electric field also provides

193   sufficient energy in the appropriate time to improve the resolutions of positive and

194   negative ions. The mass resolutions of the positive (> 1000 at maximum half width)

195   and negative (> 2000 at maximum half width) ion spectra are then significantly

196   improved. Third, the multichannel acquisition technology is used to divide the signal

197   into two channels, detecting the high and low intensity signals simultaneously without

198   signal loss. This new acquisition technology enables a detectable dynamic signal from

199   5–20000 mV, which is approximately 40 times higher than that of SPAMS. Generally,

200   the particle size measured by HP-SPAMS ranges from 0.2 to 2.0 μm and was

201   calibrated by polystyrene latex particles before and after the sampling campaign (Li et

202   al., 2011; Li et al., 2018). The field observation result from scanning mobility particle

203   sizer (SMPS) is necessary to scale the measurements of HP-SPAMS to demonstrate

204   the authentic size distributions of specific type particles. Because the SMPS was not

205 available in this sampling campaign, thus, the size distributions of amine-containing

206 particles were not discussed here.

207 **2.3 Data analysis**

208 The size and chemical compositions of single particles obtained using the

209 HP-SPAMS were analyzed using the Computational Continuation Core (COCO)

210 toolkit in MATLAB software. According to previous studies that have utilized aerosol

211 time-of-flight mass spectrometer (ATOFMS) and SPAMS, the amine-containing

212 particles were identified by querying $^{59}(CH_3)_3N^+$, $^{74}(C_2H_5)_2NH_2^+$, $^{86}(C_2H_5)_2NCH_2^+$,

213 $^{101}(C_2H_5)_3N^+$, $^{102}(C_3H_7)_2NH_2^+$, and $^{143}(C_3H_7)_3N^+$ (Healy et al., 2015; Angelino et al.,

214 2001; Cheng et al., 2018; Zhang et al., 2012). In this work, the marker ions of

215 $^{59}(CH_3)_3N^+$, $^{74}(C_2H_5)_2NH_2^+$, and $^{86}(C_2H_5)_2NCH_2^+$ were detected as the abundant

216 species, and their particle counts and ratios in the total detected single particles are

217 shown in Table 1. Single particles containing $^{86}(C_2H_5)_2NCH_2^+$ only accounted for 3.7%

218 of total particles, which was primarily due to occasional increases on September 5

219 (Figure S2), possibly due to the outburst of special emissions, such as combustion and

220 industry. Thus, in this work, particles containing $^{59}(CH_3)_3N^+$ and $^{74}(C_2H_5)_2NH_2^+$ were

221 selected to discuss the mixing states and formation processes of the particulate amines.

222 The marker ions of $^{62}NO_3^-$, $^{97}HSO_4^-$, and $^{18}NH_4^+$ were used to identify the nitrate,

223 sulfate, and ammonium in the amine-containing particles (Zhang et al., 2012). Based

224 on field and chamber studies using SPAMS and ATOFMS, the $^{43}C_2H_3O^+$ ion was

225 identified as the representative oxygen-containing organic (Healy et al., 2015; Pratt et

226 al., 2009). The particles containing $^{26}CN^-$ and $^{42}CNO^-$ were considered to be

227 representative of the organic nitrogen-containing particles (Pratt et al., 2011). In

228 addition, the $^{73}C_3H_5O_2^-$ and $^{89}HC_2O_4^-$ ions were designated as glyoxylate and oxalate

229 markers, respectively (Cheng et al., 2017; Zhang et al., 2020). It should be noted that

230 HP-SPAMS measurements cannot provide the quantitative mass concentrations of

231 amines and related chemical species due to the size-dependent transmission

232 efficiencies of particles through aerodynamic lens and composition dependent matrix

233 effect (Cheng et al., 2018; Cheng et al., 2021; Gong et al., 2021). Currently, the

234 observational results were used to illustrate the distinct impacts of same influencing

235 factors on the behaviors of amine-containing particles.

236 **3 Results and discussion**

237 **3.1 Characteristics of amine-containing particles**

238 In this work, the amine-containing particles accounted for 32.1% of total

239 detected single particles, which was higher than in previously reported results for the

240 Pearl River Delta (PRD) region (9.4%−11.1%) and Chongqing (8.3%−12.7%), China.

241 The TMA-containing particles showed a much higher abundance in the total particles

242 (22.8%) than the DEA-containing particles (5.5%) (Table 1), which could have been

243 due to their differential emissions and atmospheric processing (Cheng et al., 2018;

244 Chen et al., 2019; Liu et al., 2020; Ge et al., 2011b). Temporal variations in

245 meteorological parameters, $PM_{2.5}$ concentration, and the count of amine-containing

246 particles are shown in Figure 1. Although the TMA- and DEA-containing particles

247 exhibited similar temporal trends at a lower particle count, their increasing peaks

248 appeared at different periods, suggesting that the reasons for their increase in the

249 particle count were different. Generally, peaks in the DEA-containing particles

250 frequently appeared during the nighttime, which was possibly due to their enhanced

251 source emissions and/or favorable nighttime production (Tang et al., 2013). The

252 ambient RH was relatively high during the entire sampling period ($74 \pm 14\%$),

253 especially from September 5–7, when the count of TMA-containing particles sharply

254 increased. However, no obvious enhancement in DEA-containing particles count was

255 found, which suggested other influencing factors on their formation process in

256 addition to the ambient RH.

257 Additionally, the periods of high concentration of the amine-containing particles

258 were not consistent with the increase in $PM_{2.5}$ concentration, which could have been

259 due to the integrated effects of the emission sources and the secondary formation

260 processes. The gaseous TMA and DEA are mainly from agriculture, industry, vehicle

261 exhaust, biomass combustion, biological, and marine sources (Zhou et al., 2019;

262 Hemmilä et al., 2018; Sintermann et al., 2014; Ge et al., 2011b; Zhang et al., 2017).

263   Their concentrations vary greatly depending on the influence of source strength near

264   the sampling site. For example, the gaseous concentration of DEA was 14 and 2-5

265   times higher than TMA in polluted urban areas in China (Yao et al., 2016) and US

266   (You et al., 2014), respectively, while higher concentration of TMA than DEA was

267   observed in the forest site (You et al., 2014). Both the online and offline

268   measurements are difficult to quantitatively resolve their emission sources (You et al.,

269   2014; Yao et al., 2016; Kieloaho et al., 2013; Hellén et al., 2014). Here the backward

270   trajectories of the air masses from sampling site were discussed to explorer their

271   possible different sources. The backward trajectories of the air masses (48 h, 500 m)

272   associated with the spatial distributions of the two amine-containing particles during

273   the entire sampling period (Figure 2). More than 70% of the air masses (Clusters 1

274   and 4) were from east of the sampling site, which were both connected with

275   anthropogenic emissions in the YRD and marine sources in the East China Sea.

276   TMA-containing particles were primarily from the air masses of Cluster 1 and Cluster

277   4, while the DEA-containing particles were associated with the air masses of Cluster 3

278   and Cluster 4, which underwent long-range transport. These results suggested

279   potential different emission sources and atmospheric formation processes of TMA-

280   and DEA-containing particles, which was further investigated by examining their

281   mixing states.

282   Diurnal variations of TMA- and DEA-containing particles are shown in Figure 3.

283   The particle count of TMA-containing particles and their abundance in the total

284   particles   exhibited   identical   variation   patterns.   According   to   molecular

285   characterization of particles from vehicle exhaust, TMA was detected as one of the

286   directly emitted organics from vehicle exhaust (Zhang et al., 2017; Li et al., 2020),

287   which was in accordance with the field studies conducted during traffic hours (Cheng

288   et al., 2018; Chen et al., 2019). Thus, the significant increase of TMA-containing

289   particles in the morning was possibly associated with direct emissions from vehicle

290   exhaust. The DEA-containing particles showed a completely different diurnal pattern

291   compared with the TMA-containing particles. DEA-containing particles increased

292   during   nighttime,   but   sharply   decreased   during   the   afternoon,   when   the

293   photochemistry was the most active. The nighttime increase could have been due to

294   the high ambient RH and/or enhanced heterogeneous reactions (Zhou et al., 2019;

295   Huang et al., 2012; Zhang et al., 2019). However, since the increase in the

296   DEA-containing particles was not prominent under high RH (Figure 1), enhanced

297   heterogeneous production of particulate DEA could be a more reasonable explanation.

298   The decrease in the DEA-containing particles during the afternoon could have been

299   associated with the photodegradation of DEA and/or repartitioning of particulate DEA

300   under high temperatures during the day (Ge et al., 2011a; Pitts et al., 1978; Murphy et

301   al., 2007). In order to investigate the impact of RH on the formation process of

302   amine-containing particles, the particle counts of amine particles and the relative peak

303   areas (RPAs) of amines in the particles with an increase in the RH are presented in

304   Figure 4. The particle count of TMA-containing particles and the RPA of the TMA

305   showed remarkable increasing trends with an enhancement in RH during the entire

306   sampling period. This result suggested a significant role of RH in the formation of

307   particulate TMA. This was consistent with a field study conducted in Guangzhou,

308   China, which also found an instant increase in TMA-containing particles after the

309   occurrence of fog events (Zhang et al., 2012). In contrast, the particle count of

310   DEA-containing particles only exhibited increased RH range between 70–80% and

311   decreased with the continuous increase in the RH. Additionally, the RPA of the DEA

312   showed little change with an increase in the RH, which suggested the minor influence

313   of a change in RH on the formation of particulate DEA. The different responses of

314   TMA and DEA with RH changes signified their different formation processes in the

315   particles.

316   **3.2 Different mixing states of amine-containing particles**

317   It is important to understand the chemical compositions of amine-containing

318   particles in order to understand their mixing states and track their formation processes.

319   Hence, the positive and negative mass spectra of the amine-containing particles are

320   shown in Figure 5. Generally, TMA- and DEA-containing particles both contained

321   organic fragments such as $^{27}C_2H_3^+$, $^{37}C_3H^+$, $^{43}C_2H_3O^+$, $^{51}C_4H_3^+$, and $^{61}C_5H^+$ in the

322   positive mass spectra. In addition, their negative mass spectra were both characterized

323   by nitrate, sulfate, and nitric acid ($^{125}H(NO_3)_2^-$). However, DEA-containing particles

324   contained many more organic fragments and a higher abundance of hydrocarbon

325   clusters than the TMA-containing particles. In the positive mass spectra, the

326   abundance of the hydrocarbon fragments with an m/z below 60 was 2–3 times higher

327   in DEA-containing particles than that in TMA-containing particles. In addition,

328   hydrocarbon fragments with an m/z above 60 were barely detectable in

329   TMA-containing particles, while abundant hydrocarbon fragments with an m/z

330   ranging from 60–150 were observed in DEA-containing particles. Furthermore, the

331   DEA-containing particles also contained abundant secondary organic marker ions,

332   including organic nitrogen ($^{26}CN^-$ and $^{42}CNO^-$), acetate ($^{59}C_2H_3O_2^-$), glyoxylate

333   ($^{73}C_3H_5O_2^-$), and oxalate ($^{89}HC_2O_4^-$) in the negative mass spectra, and these were not

334   found in the TMA-containing particles. This was in accordance with the linear

335   regressions between these secondary organic ions containing particles with two

336   amine-containing particles (Table 2), which showed no correlations in the

337   TMA-containing particles ($r^2 < 0.1$), but good correlations in the DEA-containing

338   particles ($r^2 > 0.57$). The differential mass spectral features in the distributions of

339   organics in the two amine-containing particles (Figure 6) suggested that more

340   secondary organics accumulated in DEA-containing particles than in TMA-containing

341   particles. This result also implied that multiple factors influenced the mixing state of

342   DEA-containing particles in addition to ambient RH.

343   In order to further characterize the mixing states of DEA-containing particles

344   with secondary organic ions, temporal variations and diurnal patterns of secondary

345   organic ions in the DEA-containing particles are presented in Figure 7. As the

346   oxidation products of various organics, the abundances of glyoxylate and oxalate

347   commonly increased between 12:00 and 18:00 (Figure 7), when the photochemistry

348   was most active during the daytime. This result suggested the deep photochemical

349   aging state of DEA-containing particles. This might explain the decrease in the

350   particle counts of DEA-containing particles (Figure 3), which was partially associated

351   with the photo-degradation of particulate DEA. Pitts et al. (1978) reported that under

352   sunlight particulate DEA decomposed to acetamide, while DEA in the gas phase was

353   oxidized to acetaldehyde, PAN, amide, and imine. Gaseous DEA can be oxidized into

354   carbonyl compounds and other amines by ozone and OH radicals that primarily

355   include acetaldehyde and N-ethylethanimine (Tuazon et al., 2011; Tong et al., 2020).

356   The organic nitrogen markers of $^{26}CN^-$ and $^{42}CNO^-$ showed different temporal trends

357   with glyoxylate and oxalate. Although the abundances of organic nitrogen markers

358   also increased after 12:00 like oxalate, the markers still maintained high abundances

359   during the nighttime, when glyoxylate and oxalate sharply decreased. This result

360   suggested that the aging process of organics during the nighttime was slower than that

361   during the afternoon in the DEA-containing particles. Thus, the increase of

362   DEA-containing particles (Figure 3) could have been due to the enhanced production

363   of particulate DEA during the nighttime. In addition, the differential mass spectra of

364   DEA-containing particles (Figure 8) between the nighttime (22:00–02:00) and

365   daytime (14:00–18:00) showed a significant enrichment of nitrate during the

366   nighttime. This result suggested that nighttime production of particulate DEA was

367   associated with gaseous HNO_3 and/or particulate nitrate (Price et al., 2016).

368   Temporal variations in NOx and the N_f of the DEA-containing particles in the

369   total detected particles are presented in Figure 9. They showed similar increasing

370   patterns during the nighttime, and a high abundance of nitrate in the DEA-containing

371   particles was also observed. This result suggested the important role of nitrate in the

372   formation of particulate DEA. The particulate DEA during the nighttime could have

373   been produced from the reaction of gaseous DEA with HNO_3 during the gas phase

374   (R1) followed by the gas to particle partitioning (R2) and/or the direct heterogeneous

375   formation pathway (R3) (Price et al., 2016; Nielsen et al., 2012). The high ambient

376   concentration of NOx is favorable for the production of NO_3 radicals and the

377   heterogeneous production of nitrate, which might explain the distinct enhancement of

378   the DEA-containing particles. However, the same formation pathways were also

379   applied to TMA, yet there was no significant increase in the N_f of the

380   TMA-containing particles in the total particles (Figure 3). This could have been due to

381   the different particle/gas dissociation constant (K_p) for DEA·HNO_3 and TMA·HNO_3,

382   which was several orders of magnitude lower than that for DEA·HNO_3 (7.01E-09)

383   compared with TMA·HNO$_3$ (1.65E-06) at 25 ℃ (Price et al., 2016; Ge et al., 2011a).

384   During the entire sampling period, the ambient temperature during the nighttime was

385   approximately 24 ℃. Thus, the produced DEA·HNO$_3$ tended to stay in the particles,

386   while a portion of the TMA·HNO$_3$ repartitioned back into the gas phase. This resulted

387   in an insignificant increase in the TMA-containing particles. Further studies should

388   consider the influence of the different volatilities of DEA·HNO$_3$ and TMA·HNO$_3$ on

389   the formation of particulate amines in chamber experiments due to the lack of

390   quantitative results in this study.

391         $(CH_3CH_2)_2NH_{(g)} + HNO_{3(g)} \rightarrow (CH_3CH_2)_2N \cdot HNO_{3(g)}.$ (R1)

392         $(CH_3CH_2)_2N \cdot HNO_{3(g)} \leftrightarrow (CH_3CH_2)_2N \cdot HNO_{3(s)}.$ (R2)

393         $(CH_3CH_2)_2NH_{(g)} + NO_3^-{}_{(s)} \rightarrow (CH_3CH_2)_2N \cdot HNO_{3(s)}.$ (R3)
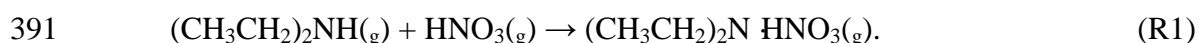
394 **3.3 Formation of aminium salts**

395   To study the acid-base reactions of TMA and DEA with sulfate and nitrate, the

396   N_fs of nitrate-, sulfate-, and ammonium-containing particles in total detected particles

397   and amine-containing particles are shown in Table 3. More than 80% of TMA- and

398   DEA-containing particles internally mixed with nitrate, which was higher than the N_f

399   of nitrate in the total particles (72%). Interestingly, the N_f of sulfate in

400   DEA-containing particles (79.3%) was much higher than that in TMA-containing

401   particles (55.3%) and in the total particles (60.1%). This was similar to a study

402   performed by Lian et al. (2020) that found a stronger correlation between

403     $^{86}(C_2H_5)_2NCH_2^+$ with sulfate than that between TMA and sulfate. In addition, in this

404   work, robust linear correlations ($r^2 > 0.9$) between nitrate-containing particles and

405   amine particles were both observed in TMA- and DEA-containing particles (Table 2).

406   However, a weak linear correlation ($r^2 = 0.32$) was found between the

407   sulfate-containing particles and the TMA-containing particles, while a better linear

408   correlation ($r^2 = 0.86$) was observed in the DEA-containing particles. According to

409   reported studies, the vapor pressure of diethylaminium sulfate (DEAS) ($0.2*10^{-12}$–

410     $12.8*10^{-12}$ Pa) was three orders of magnitude lower than that of trimethylaminium

411   sulfate (TMAS) ($0.6*10^{-9}$–$1.8*10^{-9}$ Pa) at 298 k. In addition, the enthalpy of

412   evaporation was higher than that of TMAS (DEAS: 168 ± 5 kJ mol^{-1}; TMAS: 114 ± 2

413 kJ mol^{-1}) (Lavi et al., 2013). Therefore, the thermo-stability of DEAS was stronger

414 than TMAS (Qiu and Zhang, 2012), which led to the higher N_f of sulfate in the

415 DEA-containing particles than in the TMA-containing particles.

416   The N_f of ammonium in DEA-containing particles (13.2%) was lower than in

417 TMA-containing particles (35%) and total particles (19.4%). The low abundance of

418 NH_4^+ in DMA-containing particles had been observed in our previous studies in the

419 PRD region (Cheng et al., 2018), which was partially attributed to the

420 ammonium-amine exchange reactions in the particles. The related laboratory

421 experiments primarily involved the preferential uptake of LMW amines in the H_2SO_4

422 particles (Sauerwein and Chan, 2017; Chan and Chan, 2013; Chu and Chan, 2017). In

423 this work, the distinct low N_f of NH_4^+ in the DEA particles suggested the possible

424 displacement of NH_4^+ by DEA. Moreover, the higher abundance of sulfate in DEA

425 particles than in TMA particles was more favorable for the occurrence of

426 ammonium-amine exchange reactions in DEA particles. This disparity could imply

427 differential roles of DEA and TMA in the new particle formation process (Wang et al.,

428 2010; Yin et al., 2011; Zhao et al., 2011).

429   The temporal trends of the N_fs of nitrate-, sulfate-, and ammonium-containing

430 particles in TMA and DEA particles are shown in Figure 10. The N_f of

431 nitrate-containing amine particles exhibited similar variation patterns with each type

432 of amine particle, while the N_f of sulfate-containing amine particles only showed a

433 similar variation pattern with DEA-containing particles. Although aminium nitrate

434 and sulfate salts were both produced in TMA- and DEA-containing particles, the

435 different temporal trends of sulfate and nitrate in the two amine particles suggested

436 that both sulfate and nitrate DEA salts existed in the DEA-containing particles, while

437 nitrate TMA salt dominated in TMA-containing particles (Cheng et al., 2018; Pratt et

438 al., 2009). This difference in the form of aminium salts could signify the potential

439 different influences in the hygroscopic property of secondarily processed particles

440 internally mixing with different amines (Rovelli et al., 2017; Clegg et al., 2013; Lavi

441 et al., 2013). The relative acidity ratio (Ra), defined as the ratio of the sum of the

442 sulfate and nitrate peak areas to the ammonium peak area, has been proposed in field

443   studies that use single particle mass spectrometry to roughly estimate particle acidity

444   (Huang et al., 2013; Cheng et al., 2018). Although the feasibility of Ra has been

445   supported by the robust linear correlation with authentic particle acidity calculated

446   from mass concentrations of inorganic ions   (Huang et al., 2013), this

447   semi-quantitative approach should be carefully treated when it comes to the

448   discussion about the actual acidity of atmospheric particles. In this work, temporal

449   variations in Ra in TMA-containing particles (Ra_1) and DEA-containing particles (Ra_2)

450   are shown in Figure 11. The average Ra_1 was 6.3 $\pm$1.8 in TMA-containing particles,

451   and Ra_2 was 36.1 $\pm$ 21.8 in DEA-containing particles. This result could suggest a

452   more acidic nature of DEA particles than TMA particles. However, after including the

453   peak area of amines (TMA/DEA) in the calculation of Ra, the new Ra′ reduced to 2.1

454    $\pm$ 0.5 in the TMA-containing particles and 6.5 $\pm$ 1.2 in the DEA-containing particles.

455   The gap of Ra between the two amine particles significantly decreased after including

456   amines in the calculation. The larger reduction ratio of Ra′ in DEA-containing

457   particles than in TMA-containing particles suggested the effective buffering effect of

458   amines under the absence of ammonium in the particles.

459   **3.4 Implications of the diverse mixing states of amines particles**

460   The mixing states and formation processes of the two amine-containing particles

461   were investigated under the same atmospheric environment, and their different

462   atmospheric behaviors against the same influencing factors suggested their

463   differential contributions to SOA mass. The prominent impact of ambient RH on the

464   formation of particulate TMA suggested a significant role for gas-particle partitioning

465   process to the high water-soluble species in the SOA. However, the slight influence of

466   RH on the formation of the particulate DEA implied the inconsistent role of high RH

467   on the same group of water-soluble organic molecules. In addition, the distinct

468   distribution patterns of secondary organic species in two amine-containing particles

469   also signified that the mixing states of the OA are important to explore their formation

470   processes. Furthermore, the heterogeneous processing of the DEA-containing

471   particles during the nighttime and the photochemical degradation of the DEA during

472   the daytime both generated more fractions of nitrogen- and oxygen-containing species

473   in the particles than in the TMA-containing particles. This result suggested different

474   roles of particulate TMA and DEA in the evolution of hygroscopicity and aging state

475   of the SOA. In summary, understanding mixing states and formation processes of

476   different amines in single particles is of great significance to reveal the unique

477   response of each type of amine to the same atmospheric environment. Single-particle

478   analysis provided insights into the mixing states of specific organic species to further

479   understand the formation process of the SOA.

480   **4 Summary and conclusions**

481   TMA- and DEA-containing single particles were collected and analyzed on

482   September 2019 using HP-SPAMS in Nanjing, China, and accounted for 22.8% and

483   5.5% of total detected particles, respectively. The mixing states and formation

484   processes of TMA- and DEA-containing particles were studied. With increased RH,

485   the counts of particulate TMA and the RPA of the TMA displayed an obvious upward

486   trend, while the particle count of the particulate DEA slightly increased when the RH

487   was 70–80%. In addition, the RPA of the DEA showed no difference in reaction to

488   RH change during the entire sampling period. This suggested a differential role for

489   ambient RH during the formation processes of particulate TMA and DEA. The

490   possible formation processes were further evaluated by analyzing the mixing states of

491   the amine-containing particles. The mass spectra of the amine-containing particles

492   showed that the secondary organic species were enriched in the DEA-containing

493   particles. The differential distributions of the secondary ions effectively explained the

494   sharp increase in DEA-containing particles during the nighttime, which could have

495   been due to the heterogeneous reactions of gaseous DEA with HNO_3 and/or nitrate

496   particles. The prominent decrease in the DEA-containing particles during the

497   afternoon was attributed to photo-degradation of particulate DEA. Due to the

498   differences in the thermodynamic properties, the N_f of sulfate in the particulate DEA

499   was higher than that in the particulate TMA. The amine-ammonium exchange

500   reaction resulted in particulate DEA containing less NH_4^+. In addition, the particulate

501   DEA was abundant in sulfate, which was more favorable for the exchange of amine

502 and ammonium. The higher relative acidity ratio in DEA-containing particles relative

503 to TMA-containing particles could suggest that DEA particles are more acidic. After

504 including the peak area of amines (TMA/DEA) in the calculation, the larger reduction

505 ratio of the Ra′ in DEA-containing particles than in TMA-containing particles

506 suggested the effective buffering effect of amines under the absence of ammonium in

507 the particles. These results revealed the distinct mixing states and chemical behaviors

508 of TMA- and DEA-containing single particles and could imply a potential role for

509 DEA as an indicator of the OA aging process.

510

511 **Data availability**

512 The observational data, including HP-SPAMS and the meteorological parameters,

513 obtained in this study are available from the corresponding authors upon request

514 (chengcl@jnu.edu.cn).

515

516 **Author contribution**

517 **Qi En Zhong, Chunlei Cheng, Zaihua Wang:** methodology, writing original

518 draft. **Dafeng Ge, Lei Wang, Yuanyuan Li, Wei Nie, Xuguang Chi, Aijun Ding:**

519 methodology, sampling. **Lei Li, Mei Li, Suxia Yang, Duohong Chen, Zhen Zhou:**

520 providing discussions and helping to revise original draft.

521

522 **Competing interests**

523 I declare that I or my co-authors have competing interests as follows: Aijun Ding

524 is editor of ACP.

525

526 **Acknowledgements**: This work was financially supported by the National Key

527 Research and Development Program of China (Grant No. 2018 YFE0106900), the

528 National Natural Science Foundation of China (Grant Nos. 41805093, 41827804 and

529 41875175), the NSFC of Guangdong Province (Grant No. 2021A1515011206), the

Guangzhou Economic and Technological Development District International Science and Technology Cooperation Project (Grant No. 2018GH08), the National Research Program for Key Issues in Air Pollution Control (Grant No. DQGG0107), the Pearl River Nova Program of Guangzhou (No. 201806010064), and GDAS' Project of Science and Technology Development (2021GDASYL-20210103058).

References

Angelino, S., Suess, D. T., and Prather, K. A.: Formation of aerosol particles from reactions of secondary and tertiary alkylamines: characterization by aerosol time-of-flight mass spectrometry, Environmental science & technology, 35, 3130-3138, 10.1021/es0015444, 2001.

Berndt, T., Stratmann, F., Sipilä, M., Vanhanen, J., Petäjä, T., Mikkilä, J., Grüner, A., Spindler, G., Lee Mauldin Iii, R., Curtius, J., Kulmala, M., and Heintzenberg, J.: Laboratory study on new particle formation from the reaction OH +SO2: influence of experimental conditions, H2O vapour, NH3 and the amine tert-butylamine on the overall process, Atmospheric Chemistry and Physics, 10, 7101-7116, 10.5194/acp-10-7101-2010, 2010.

Chan, L. P. and Chan, C. K.: Role of the aerosol phase state in ammonia/amines exchange reactions, Environmental science & technology, 47, 5755-5762, 10.1021/es4004685, 2013.

Chen, Y., Kozlovskiy, V., Du, X., Lv, J., Nikiforov, S., Yu, J., Kolosov, A., Gao, W., Zhou, Z., Huang, Z., and Li, L.: Increase of the particle hit rate in a laser single-particle mass spectrometer by pulse delayed extraction technology, Atmospheric Measurement Techniques, 13, 941-949, 10.5194/amt-13-941-2020, 2020.

Chen, Y., Tian, M., Huang, R.-J., Shi, G., Wang, H., Peng, C., Cao, J., Wang, Q., Zhang, S., Guo, D., Zhang, L., and Yang, F.: Characterization of urban amine-containing particles in southwestern China: seasonal variation, source, and processing, Atmospheric Chemistry and Physics, 19, 3245-3255, 10.5194/acp-19-3245-2019, 2019.

Cheng, C., Chan, C. K., Lee, B. P., Gen, M., Li, M., Yang, S., Hao, F., Wu, C., Cheng, P., Wu, D., Li, L., Huang, Z., Gao, W., Fu, Z., and Zhou, Z.: Single particle diversity and mixing state of carbonaceous aerosols in Guangzhou, China, The Science of the total environment, 754, 142182, 10.1016/j.scitotenv.2020.142182, 2021.

Cheng, C., Huang, Z., Chan, C. K., Chu, Y., Li, M., Zhang, T., Ou, Y., Chen, D., Cheng, P., Li, L., Gao, W., Huang, Z., Huang, B., Fu, Z., and Zhou, Z.: Characteristics and mixing state of amine-containing particles at a rural site in the Pearl River Delta, China, Atmospheric Chemistry and Physics, 18, 9147-9159, 10.5194/acp-18-9147-2018, 2018.

Cheng, C., Li, M., Chan, C. K., Tong, H., Chen, C., Chen, D., Wu, D., Li, L., Wu, C., Cheng, P., Gao, W., Huang, Z., Li, X., Zhang, Z., Fu, Z., Bi, Y., and Zhou, Z.: Mixing state of oxalic acid containing particles in the rural area of Pearl River Delta, China: implications for the formation mechanism of oxalic acid, Atmospheric Chemistry and Physics, 17, 9519-9533, 10.5194/acp-17-9519-2017, 2017.

Chu, Y. and Chan, C. K.: Reactive Uptake of Dimethylamine by Ammonium Sulfate and Ammonium Sulfate-Sucrose Mixed Particles, The journal of physical chemistry. A, 121, 206-215, 10.1021/acs.jpca.6b10692, 2017.

Chu, Y., Sauerwein, M., and Chan, C. K.: Hygroscopic and phase transition properties of alkyl aminium sulfates at low relative humidities, Physical chemistry chemical physics : PCCP, 17, 19789-19796, 10.1039/c5cp02404h, 2015.

Clegg, S. L., Qiu, C., and Zhang, R.: The deliquescence behaviour, solubilities, and densities of aqueous solutions of five methyl- and ethyl-aminium sulphate salts, Atmospheric Environment, 73, 145-158, 10.1016/j.atmosenv.2013.02.036, 2013.

Ding, A., Nie, W., Huang, X., Chi, X., Sun, J., Kerminen, V.-M., Xu, Z., Guo, W., Petäjä, T., Yang, X., Kulmala, M., and Fu, C.: Long-term observation of air pollution-weather/climate interactions at the SORPES station: a review and outlook, Frontiers of Environmental Science & Engineering, 10, 10.1007/s11783-016-0877-3, 2016.

Ding, A. J., Fu, C. B., Yang, X. Q., Sun, J. N., Zheng, L. F., Xie, Y. N., Herrmann, E., Nie, W., Petäjä, T., Kerminen, V. M., and Kulmala, M.: Ozone and fine particle in the western Yangtze River Delta: an overview of 1 yr data at the SORPES station, Atmospheric Chemistry and Physics, 13, 5813-5830, 10.5194/acp-13-5813-2013, 2013a.

Ding, A. J., Fu, C. B., Yang, X. Q., Sun, J. N., Petäjä, T., Kerminen, V. M., Wang, T., Xie, Y., Herrmann, E., Zheng, L. F., Nie, W., Liu, Q., Wei, X. L., and Kulmala, M.: Intense atmospheric pollution modifies weather: a case of mixed biomass burning with fossil fuel combustion pollution in eastern China, Atmospheric Chemistry and Physics, 13, 10545-10554, 10.5194/acp-13-10545-2013, 2013b.

Facchini, M. C., Decesari, S., Rinaldi, M., Carbone, C., Finessi, E., Mircea, M., Fuzzi, S., Moretti, F., Tagliavini, E., Ceburnis, D., and O'Dowd, C. D.: Important source of marine secondary organic aerosol from biogenic amines, Environmental science & technology, 42, 9116-9121, 10.1021/es8018385, 2008.

Ge, X., Wexler, A. S., and Clegg, S. L.: Atmospheric amines – Part II. Thermodynamic properties and gas/particle partitioning, Atmospheric Environment, 45, 561-577, 10.1016/j.atmosenv.2010.10.013, 2011a.

Ge, X., Wexler, A. S., and Clegg, S. L.: Atmospheric amines – Part I. A review, Atmospheric Environment, 45, 524-546, 10.1016/j.atmosenv.2010.10.012, 2011b.

Gong, H., Cheng, C., Li, M., Yang, S., Zhou, Q., Zhong, Q. E., Zhang, Y., Xie, Y., and Zhou, Z.: The enhanced mixing states of oxalate with metals in single particles in Guangzhou, China, The Science of the total environment, 783, 146962, 10.1016/j.scitotenv.2021.146962, 2021.

614 Healy, R. M., Evans, G. J., Murphy, M., Sierau, B., Arndt, J., McGillicuddy, E.,
615   O'Connor, I. P., Sodeau, J. R., and Wenger, J. C.: Single-particle speciation of
616   alkylamines in ambient aerosol at five European sites, Analytical and
617   bioanalytical chemistry, 407, 5899-5909, 10.1007/s00216-014-8092-1, 2015.
618 Hellén, H., Kieloaho, A. J., and Hakola, H.: Gas-phase alkyl amines in urban air;
619   comparison with a boreal forest site and importance for local atmospheric
620   chemistry, Atmospheric Environment, 94, 192-197,
621   10.1016/j.atmosenv.2014.05.029, 2014.
622 Hemmilä, M., Hellén, H., Virkkula, A., Makkonen, U., Praplan, A. P., Kontkanen, J.,
623   Ahonen, L., Kulmala, M., and Hakola, H.: Amines in boreal forest air at SMEAR
624   II station in Finland, Atmospheric Chemistry and Physics, 18, 6367-6380,
625   10.5194/acp-18-6367-2018, 2018.
626 Huang, Y., Chen, H., Wang, L., Yang, X., and Chen, J.: Single particle analysis of
627   amines in ambient aerosol in Shanghai, Environmental Chemistry, 9, 202,
628   10.1071/en11145, 2012.
629 Huang, Y., Li, L., Li, J., Wang, X., Chen, H., Chen, J., Yang, X., Gross, D. S., Wang,
630   H., Qiao, L., and Chen, C.: A case study of the highly time-resolved evolution of
631   aerosol chemical and optical properties in urban Shanghai, China, Atmospheric
632   Chemistry and Physics, 13, 3931-3944, 10.5194/acp-13-3931-2013, 2013.
633 Kieloaho, A.-J., Hellén, H., Hakola, H., Manninen, H. E., Nieminen, T., Kulmala, M.,
634   and Pihlatie, M.: Gas-phase alkylamines in a boreal Scots pine forest air,
635   Atmospheric Environment, 80, 369-377, 10.1016/j.atmosenv.2013.08.019, 2013.
636 Lavi, A., Bluvshtein, N., Segre, E., Segev, L., Flores, M., and Rudich, Y.:
637   Thermochemical, Cloud Condensation Nucleation Ability, and Optical
638   Properties of Alkyl Aminium Sulfate Aerosols, The Journal of Physical
639   Chemistry C, 117, 22412-22421, 10.1021/jp403180s, 2013.
640 Li, L., Liu, L., Xu, L., Li, M., Li, X., Gao, W., Huang, Z., and Cheng, P.:
641   Improvement in the Mass Resolution of Single Particle Mass Spectrometry
642   Using Delayed Ion Extraction, Journal of the American Society for Mass
643   Spectrometry, 29, 2105-2109, 10.1007/s13361-018-2037-4, 2018.
644 Li, L., Huang, Z., Dong, J., Li, M., Gao, W., Nian, H., Fu, Z., Zhang, G., Bi, X.,
645   Cheng, P., and Zhou, Z.: Real time bipolar time-of-flight mass spectrometer for
646   analyzing single aerosol particles, International Journal of Mass Spectrometry,
647   303, 118-124, 10.1016/j.ijms.2011.01.017, 2011.
648 Li, W., Liu, L., Zhang, J., Xu, L., Wang, Y., Sun, Y., and Shi, Z.: Microscopic
649   Evidence for Phase Separation of Organic Species and Inorganic Salts in Fine
650   Ambient Aerosol Particles, Environmental science & technology, 55, 2234-2242,
651   10.1021/acs.est.0c02333, 2021.
652 Li, W., Shao, L., Zhang, D., Ro, C.-U., Hu, M., Bi, X., Geng, H., Matsuki, A., Niu, H.,
653   and Chen, J.: A review of single aerosol particle studies in the atmosphere of
654   East Asia: morphology, mixing state, source, and heterogeneous reactions,
655   Journal of Cleaner Production, 112, 1330-1349, 10.1016/j.jclepro.2015.04.050,
656   2016a.

657 Li, W., Sun, J., Xu, L., Shi, Z., Riemer, N., Sun, Y., Fu, P., Zhang, J., Lin, Y., and
658   Wang, X.: A conceptual framework for mixing structures in individual aerosol
659   particles, Journal of Geophysical Research: Atmospheres, 121, 13,784-713,798,
660   2016b.

661 Li, X.-J., Shi, X.-W., Ma, Y., and Zheng, J.: Characterization, Seasonal Variation, and
662   Source Apportionments of Particulate Amines (PM$_{2.5}$) in Northern Suburb of
663   Nanjing, Huan Jing ke Xue= Huanjing Kexue, 41, 537-553, 2020.

664 Liu, Y., Nie, W., Li, Y., Ge, D., Liu, C., Xu, Z., Chen, L., Wang, T., Wang, L., and
665   Sun, P.: Formation of condensable organic vapors from anthropogenic and
666   biogenic VOCs is strongly perturbed by NOx in eastern China, Atmospheric
667   Chemistry and Physics Discussions, 1-44, 2021.

668 Liu, Z., Chen, H., Li, Q., Sun, J., Wang, L., Yang, X., Xiao, H., Li, M., and Chen, J.:
669   Size‐Resolved Mixing States and Sources of Amine‐Containing Particles in
670   the East China Sea, Journal of Geophysical Research: Atmospheres,
671   10.1029/2020jd033162, 2020.

672 Murphy, S., Sorooshian, A., Kroll, J., Ng, N., Chhabra, P., Tong, C., Surratt, J.,
673   Knipping, E., Flagan, R., and Seinfeld, J.: Secondary aerosol formation from
674   atmospheric reactions of aliphatic amines, Atmospheric Chemistry and Physics,
675   7, 2313-2337, 2007.

676 Nielsen, C. J., Bossi, R., Bunkan, A. J. C., Dithmer, L., Glasius, M., Hallquist, M.,
677   Hansen, A. M. K., Lutz, A., Salo, K., and Maguta, M. M.: Atmospheric
678   Degradation of Amines (ADA): summary report from atmospheric chemistry
679   studies of amines, nitrosamines, nitramines and amides, 2012.

680 Pitts, J. N., Grosjean, D., Van Cauwenberghe, K., Schmid, J. P., and Fitz, D. R.:
681   Photooxidation of aliphatic amines under simulated atmospheric conditions:
682   formation of nitrosamines, nitramines, amides, and photochemical oxidant,
683   Environmental science & technology, 12, 946-953, 10.1021/es60144a009, 1978.

684 Pratt, K. A., Hatch, L. E., and Prather, K. A.: Seasonal volatility dependence of
685   ambient particle phase amines, Environmental science & technology, 43,
686   5276-5281, 10.1021/es803189n, 2009.

687 Pratt, K. A., Murphy, S. M., Subramanian, R., DeMott, P. J., Kok, G. L., Campos, T.,
688   Rogers, D. C., Prenni, A. J., Heymsfield, A. J., Seinfeld, J. H., and Prather, K. A.:
689   Flight-based chemical characterization of biomass burning aerosols within two
690   prescribed burn smoke plumes, Atmospheric Chemistry and Physics, 11,
691   12549-12565, 10.5194/acp-11-12549-2011, 2011.

692 Price, D. J., Kacarab, M., Cocker, D. R., Purvis-Roberts, K. L., and Silva, P. J.:
693   Effects of temperature on the formation of secondary organic aerosol from amine
694   precursors, Aerosol Science and Technology, 50, 1216-1226,
695   10.1080/02786826.2016.1236182, 2016.

696 Price, D. J., Clark, C. H., Tang, X., Cocker, D. R., Purvis-Roberts, K. L., and Silva, P.
697   J.: Proposed chemical mechanisms leading to secondary organic aerosol in the
698   reactions of aliphatic amines with hydroxyl and nitrate radicals, Atmospheric
699   Environment, 96, 135-144, 10.1016/j.atmosenv.2014.07.035, 2014.

Qiu, C. and Zhang, R.: Physiochemical properties of alkylaminium sulfates: hygroscopicity, thermostability, and density, Environmental science & technology, 46, 4474-4480, 10.1021/es3004377, 2012.

Qiu, C., Wang, L., Lal, V., Khalizov, A. F., and Zhang, R.: Heterogeneous reactions of alkylamines with ammonium sulfate and ammonium bisulfate, Environmental science & technology, 45, 4748-4755, 10.1021/es1043112, 2011.

Rehbein, P. J., Jeong, C. H., McGuire, M. L., Yao, X., Corbin, J. C., and Evans, G. J.: Cloud and fog processing enhanced gas-to-particle partitioning of trimethylamine, Environmental science & technology, 45, 4346-4352, 10.1021/es1042113, 2011.

Rovelli, G., Miles, R. E. H., Reid, J. P., and Clegg, S. L.: Hygroscopic properties of aminium sulfate aerosols, Atmospheric Chemistry and Physics, 17, 4369-4385, 10.5194/acp-17-4369-2017, 2017.

Sauerwein, M. and Chan, C. K.: Heterogeneous uptake of ammonia and dimethylamine into sulfuric and oxalic acid particles, Atmospheric Chemistry and Physics, 17, 6323-6339, 10.5194/acp-17-6323-2017, 2017.

Silva, P. J., Erupe, M. E., Price, D., Elias, J., Malloy, Q. G., Li, Q., Warren, B., and Cocker, D. R., 3rd: Trimethylamine as precursor to secondary organic aerosol formation via nitrate radical reaction in the atmosphere, Environmental science & technology, 42, 4689-4696, 10.1021/es703016v, 2008.

Sintermann, J., Schallhart, S., Kajos, M., Jocher, M., Bracher, A., Münger, A., Johnson, D., Neftel, A., and Ruuskanen, T.: Trimethylamine emissions in animal husbandry, Biogeosciences, 11, 5073-5085, 10.5194/bg-11-5073-2014, 2014.

Sorooshian, A., Murphy, S., Hersey, S., Gates, H., Padro, L., Nenes, A., Brechtel, F., Jonsson, H., Flagan, R., and Seinfeld, J.: Comprehensive airborne characterization of aerosol from a major bovine source, Atmospheric Chemistry and Physics, 8, 5489-5520, 2008.

Tang, X., Price, D., Praske, E., Lee, S. A., Shattuck, M. A., Purvis-Roberts, K., Silva, P. J., Asa-Awuku, A., and Cocker, D. R.: NO3 radical, OH radical and O3-initiated secondary aerosol formation from aliphatic amines, Atmospheric Environment, 72, 105-112, 10.1016/j.atmosenv.2013.02.024, 2013.

Tao, Y., Ye, X., Jiang, S., Yang, X., Chen, J., Xie, Y., and Wang, R.: Effects of amines on particle growth observed in new particle formation events, Journal of Geophysical Research: Atmospheres, 121, 324-335, 10.1002/2015jd024245, 2016.

Tong, D., Chen, J., Qin, D., Ji, Y., Li, G., and An, T.: Mechanism of atmospheric organic amines reacted with ozone and implications for the formation of secondary organic aerosols, The Science of the total environment, 737, 139830, 10.1016/j.scitotenv.2020.139830, 2020.

Tuazon, E. C., Martin, P., Aschmann, S. M., Arey, J., and Atkinson, R.: Kinetics of the reactions of OH radicals with 2-methoxy-6-(trifluoromethyl)pyridine, diethylamine, and 1,1,3,3,3-pentamethyldisiloxan-1-ol at 298 ± 2 K, International Journal of Chemical Kinetics, 43, 631-638, 10.1002/kin.20594, 2011.

Wang, L., Lal, V., Khalizov, A. F., and Zhang, R.: Heterogeneous chemistry of alkylamines with sulfuric acid: Implications for atmospheric formation of alkylaminium sulfates, Environmental science & technology, 44, 2461-2465, 2010.

Xu, Z. N., Nie, W., Liu, Y. L., Sun, P., Huang, D. D., Yan, C., Krechmer, J., Ye, P. L., Xu, Z., Qi, X. M., Zhu, C. J., Li, Y. Y., Wang, T. Y., Wang, L., Huang, X., Tang, R. Z., Guo, S., Xiu, G. L., Fu, Q. Y., Worsnop, D., Chi, X. G., and Ding, A. J.: Multifunctional Products of Isoprene Oxidation in Polluted Atmosphere and Their Contribution to SOA, Geophysical Research Letters, 48, 10.1029/2020gl089276, 2021.

Yao, L., Wang, M.-Y., Wang, X.-K., Liu, Y.-J., Chen, H.-F., Zheng, J., Nie, W., Ding, A.-J., Geng, F.-H., Wang, D.-F., Chen, J.-M., Worsnop, D. R., and Wang, L.: Detection of atmospheric gaseous amines and amides by a high-resolution time-of-flight chemical ionization mass spectrometer with protonated ethanol reagent ions, Atmospheric Chemistry and Physics, 16, 14527-14543, 10.5194/acp-16-14527-2016, 2016.

Yin, S., Ge, M., Wang, W., Liu, Z., and Wang, D.: Uptake of gas-phase alkylamines by sulfuric acid, Chinese Science Bulletin, 56, 1241-1245, 10.1007/s11434-010-4331-9, 2011.

You, Y., Kanawade, V. P., de Gouw, J. A., Guenther, A. B., Madronich, S., Sierra-Hernández, M. R., Lawler, M., Smith, J. N., Takahama, S., Ruggeri, G., Koss, A., Olson, K., Baumann, K., Weber, R. J., Nenes, A., Guo, H., Edgerton, E. S., Porcelli, L., Brune, W. H., Goldstein, A. H., and Lee, S. H.: Atmospheric amines and ammonia measured with a chemical ionization mass spectrometer (CIMS), Atmospheric Chemistry and Physics, 14, 12181-12194, 10.5194/acp-14-12181-2014, 2014.

Youn, J. S., Crosbie, E., Maudlin, L. C., Wang, Z., and Sorooshian, A.: Dimethylamine as a major alkyl amine species in particles and cloud water: Observations in semi-arid and coastal regions, Atmos Environ (1994), 122, 250-258, 10.1016/j.atmosenv.2015.09.061, 2015.

Yu, H., Li, W., Zhang, Y., Tunved, P., Dall'Osto, M., Shen, X., Sun, J., Zhang, X., Zhang, J., and Shi, Z.: Organic coating on sulfate and soot particles during late summer in the Svalbard Archipelago, Atmospheric Chemistry and Physics, 19, 10433-10446, 10.5194/acp-19-10433-2019, 2019.

Zhang, G., Bi, X., Chan, L. Y., Li, L., Wang, X., Feng, J., Sheng, G., Fu, J., Li, M., and Zhou, Z.: Enhanced trimethylamine-containing particles during fog events detected by single particle aerosol mass spectrometry in urban Guangzhou, China, Atmospheric Environment, 55, 121-126, 10.1016/j.atmosenv.2012.03.038, 2012.

Zhang, G., Lian, X., Fu, Y., Lin, Q., Li, L., Song, W., Wang, Z., Tang, M., Chen, D., Bi, X., Wang, X., and Sheng, G.: High secondary formation of nitrogen-containing organics (NOCs) and its possible link to oxidized organics and ammonium, Atmospheric Chemistry and Physics, 20, 1469-1481, 10.5194/acp-20-1469-2020, 2020.

788 Zhang, H., Li, Y., Liu, K., Zhu, L., and Chen, H.: Selective molecular characterization
789   of particulate matter from gasoline cars using internal extractive electrospray
790   ionization mass spectrometry, Analytical Methods, 9, 6491-6498,
791   10.1039/c7ay02087b, 2017.
792 Zhang, J., Luo, B., Zhang, W., Rao, Z., and Song, H.: Single-particle characterization
793   of amine-containing particles during summer and winter in Chengdu, CHINA
794   ENVIRONMENTAL SCIENCECE, 39, 3152-3160, 2019.
795 Zhao, J., Smith, J. N., Eisele, F. L., Chen, M., Kuang, C., and McMurry, P. H.:
796   Observation of neutral sulfuric acid-amine containing clusters in laboratory and
797   ambient measurements, Atmospheric Chemistry and Physics, 11, 10823-10836,
798   10.5194/acp-11-10823-2011, 2011.
799 Zhao, J., Zhang, Y., Patton, A. P., Ma, W., Kan, H., Wu, L., Fung, F., Wang, S., Ding,
800   D., and Walker, K.: Projection of ship emissions and their impact on air quality
801   in 2030 in Yangtze River delta, China, Environmental pollution, 263, 114643,
802   10.1016/j.envpol.2020.114643, 2020.
803 Zhou, S., Li, H., Yang, T., Chen, Y., Deng, C., Gao, Y., Chen, C., and Xu, J.:
804   Characteristics and sources of aerosol aminiums over the eastern coast of China:
805   insights from the integrated observations in a coastal city, adjacent island and
806   surrounding marginal seas, Atmospheric Chemistry and Physics, 19,
807   10447-10467, 10.5194/acp-19-10447-2019, 2019.
808

838 **Figure 8.** Differential mass spectra of DEA-containing particles between 22:00–02:00

839 and 14:00–18:00.

840 **Figure 9.** Temporal trends of RPA nitrate in DEA-containing particles, number

841 fraction of DEA-containing particles in total particles, and NOx concentration.

842 **Figure 10.** Temporal trends of TMA- and DEA-containing particle counts, and

843 number fractions of nitrate, sulfate, and ammonium in TMA- and DEA-containing

844 particles.

845 **Figure 11.** Temporal trends of the relative acidity ratios (Ra, Ra$^{'}$) in TMA- and

846 DEA-containing particles.

847
848
849
850
851
852
853
854
855
856
857
858
859
860
861
862
863
864
865
866
867
868
869
870
871
872
873
874
875
876

Tables

Table 1. Summary of the major species of detected amine-containing particles and fragments in September in Nanjing, China.

Alkylamine assignment	Count	Percentage (%)
All detected particles	4 693 931	
$^{59}(CH_3)_3N^+$ (TMA)-containing particles	1072143	22.8
$^{74}(C_2H_5)_2NH_2^+$ (DEA) -containing particles	259913	5.5
$^{86}(C_2H_5)_2NCH_2^+$ (TEA)-containing particles	172621	3.7

Table 2. The linear correlations (r^2) between secondary ion-containing amine particles within TMA- and DEA-containing particles.

	TMA particles	DEA particles
$^{26}CN^-$	0.13	0.70
$^{42}CNO^-$	0.09	0.70
$^{73}C_3H_5O_2^-$	0.01	0.66
$^{89}HC_2O_4^-$	0.09	0.57
$^{43}C_2H_3O^+$	0.05	0.90
$^{62}NO_3^-$	0.93	0.90
$^{97}HSO_4^-$	0.32	0.86
$^{18}NH_4^+$	0.50	0.28

Table 3. Number fractions sulfate, nitrate, and ammonium in TMA-containing particles, DEA-containing particles, and total particles.

	TMA particles	DEA particles	Total particles
Sulfate	55.3	79.3	60.1
Nitrate	81.6	81.8	72.0
Ammonium	35.0	13.2	19.4

Figures

896
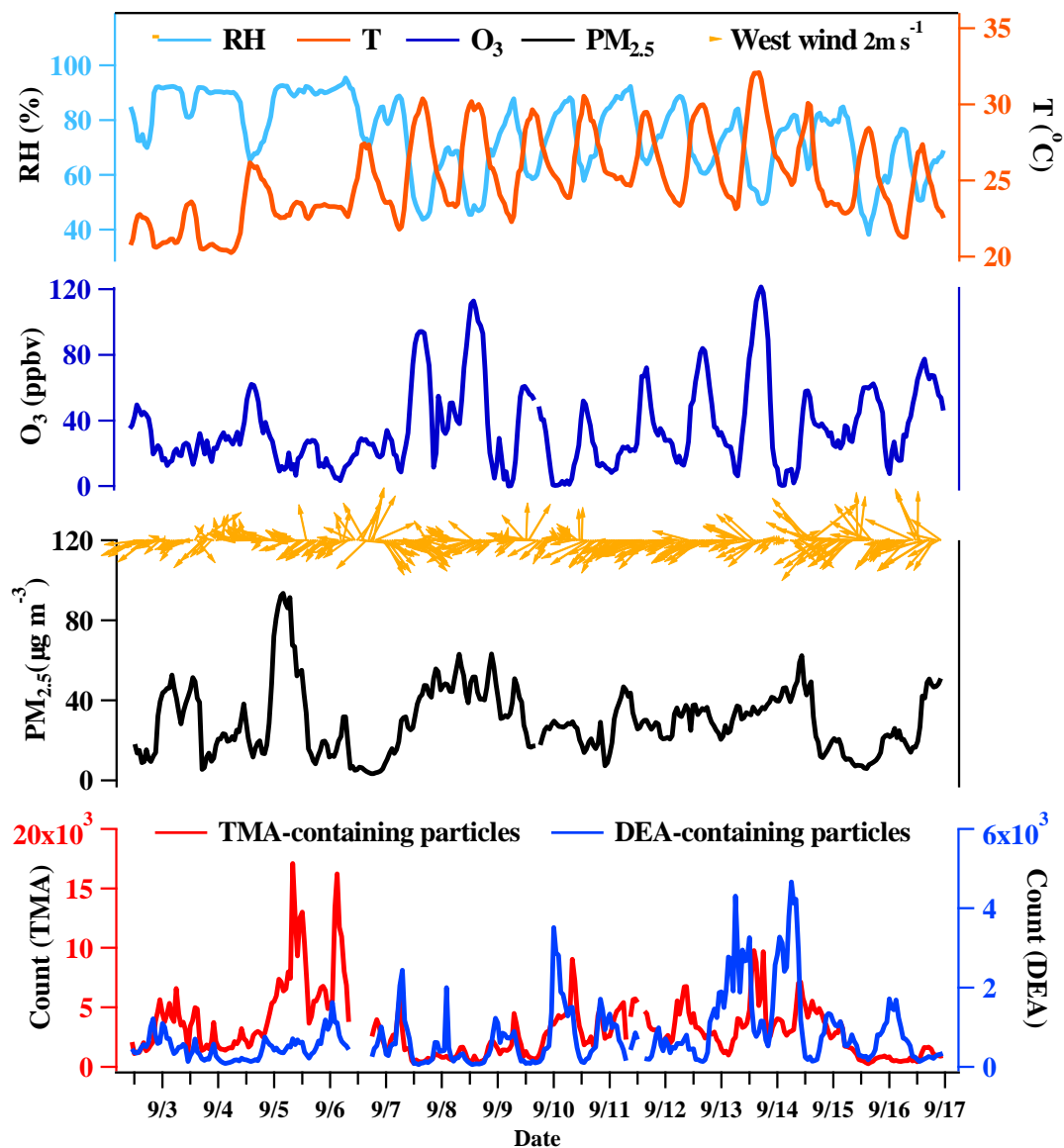
Figure 1. Temporal variations in relative humidity (RH), temperature (T), O_3 concentration, $PM_{2.5}$ concentration, wind speed, wind direction, and TMA- and DEA-containing particles during the entire sampling period.

900

901

902

903

904

905
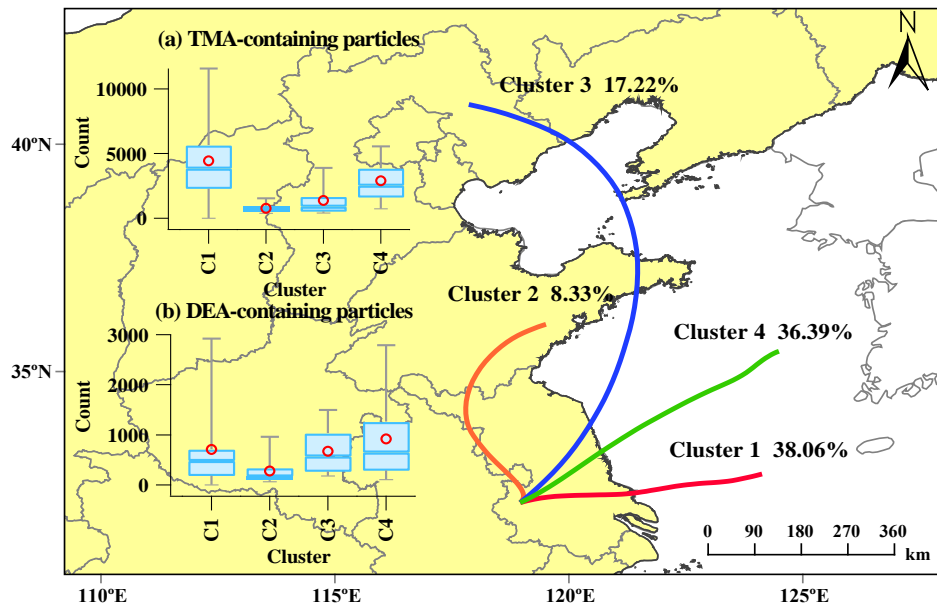
Figure 2. Backward trajectories (48 h) of air masses at 500 m above the ground during the sampling period: (a) TMA-containing particles counts; (b) DEA-containing particle counts. C1 to C4 represent cluster 1 to cluster 4.

926

927
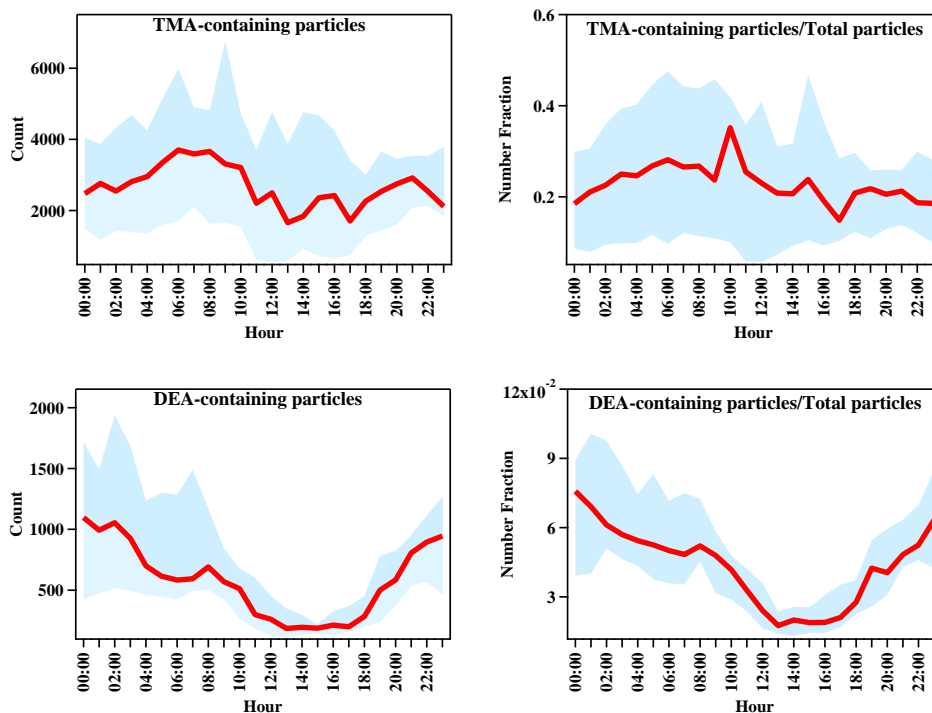
Figure 3. The diurnal variations in particle counts and number fractions of the two amine-containing particles in total particles during the entire sampling period. The shaded areas represent the 75th and 25th percentiles.

928

929

930

931

932

933

934

935

936

937

938

939

940

941

942

943

944

945

946
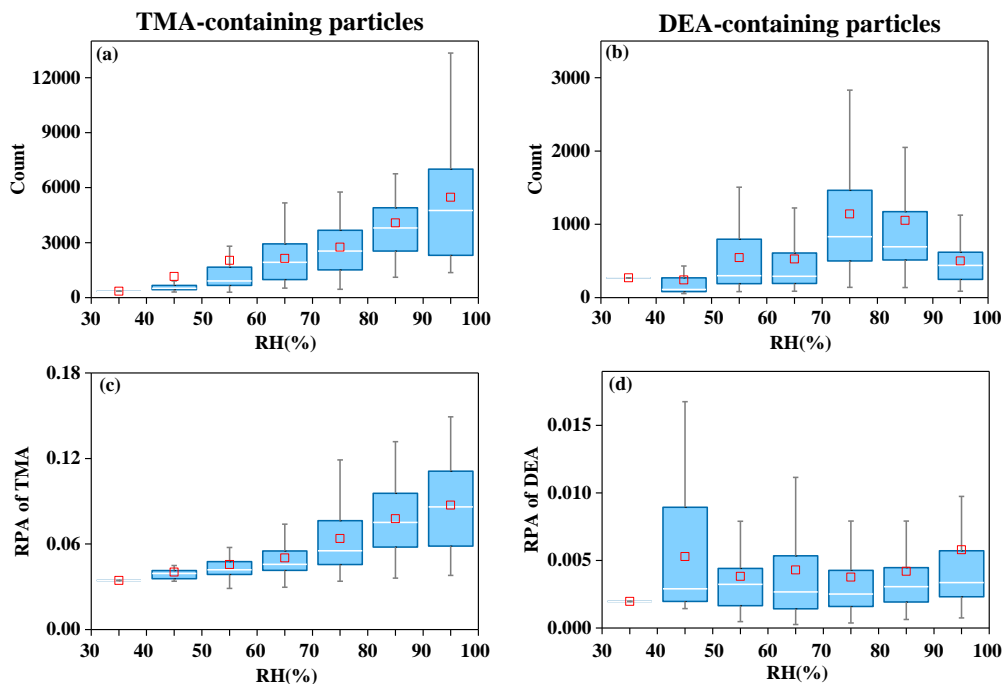
Figure 4. Particle counts of amine-containing particles and relative peak area (RPA) of the two amines in single particles, with an increase in ambient RH. (a, c) TMA-containing particles; (b, d) DEA-containing particles. Squares represent the average values. The line inside the box indicates the median. Upper and lower boundaries of the box represent the 75th and the 25th percentiles; the whiskers above and below each box represent the 95th and 5th percentiles.

953

954

955

956

957

958

959

960

961

962

963

964
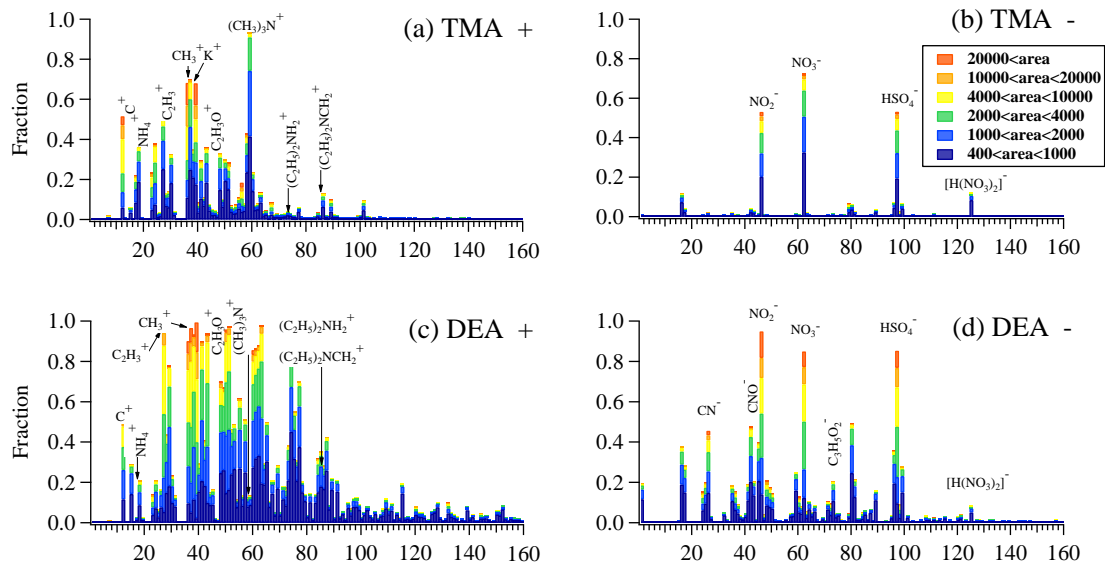
965

966 **Figure 5.** Mass spectra of TMA- and DEA-containing particles during the entire

967 sampling period.

968

969

970

971
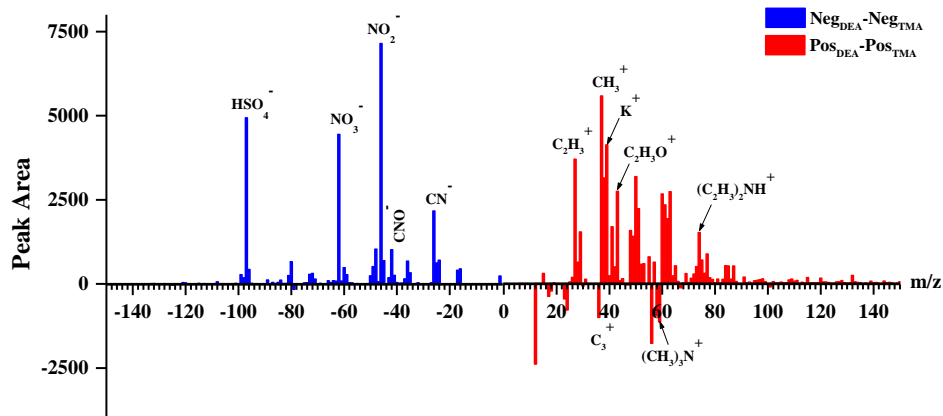
972

973 **Figure 6.** Differential mass spectra between DEA- and TMA-containing particles.

974

975

976

977

978

979

980
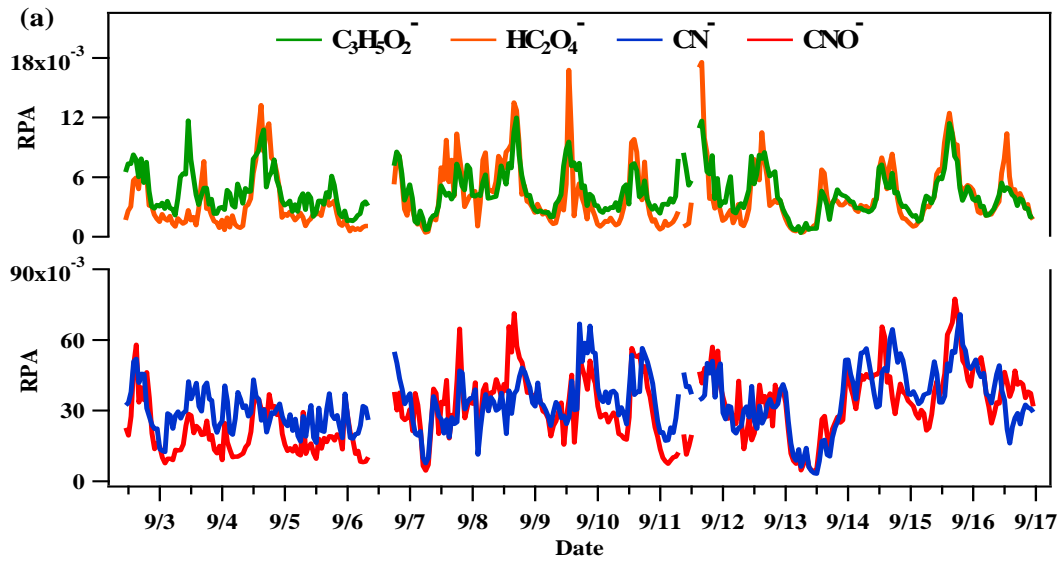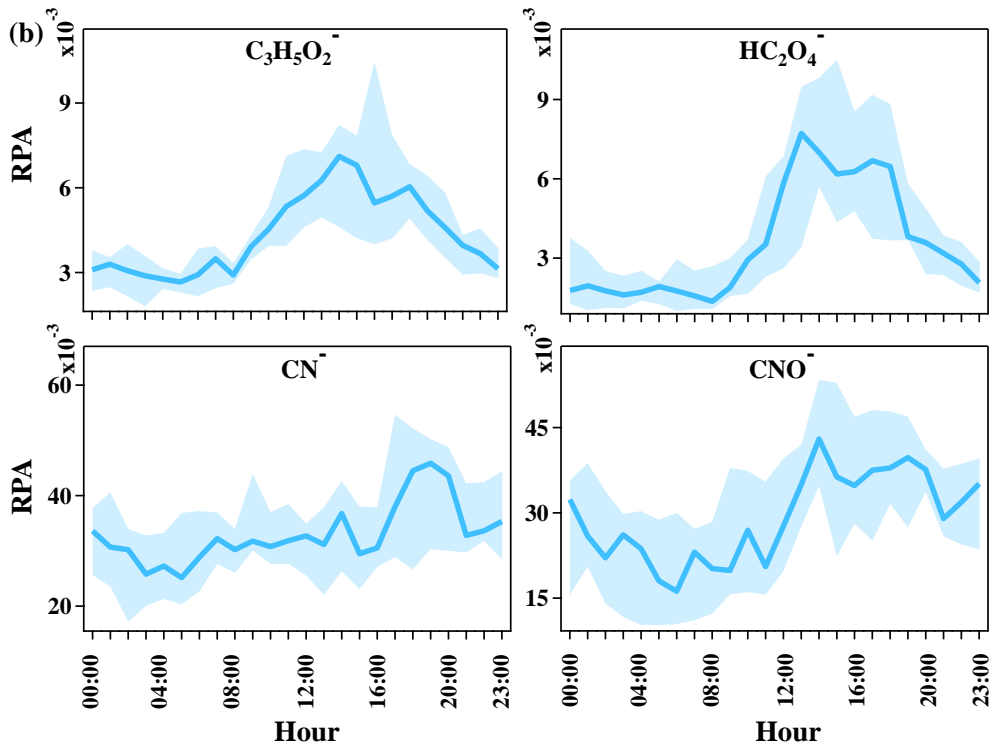
Figure 7. (a) Temporal trends of the relative peak areas (RPAs) of $^{73}C_3H_5O_2{}^-$, $^{89}HC_2O_4{}^-$, $^{26}CN^-$, and $^{42}CNO^-$ in DEA-containing particles. **(b)** Diurnal variations in the relative RPAs of $^{73}C_3H_5O_2{}^-$, $^{89}HC_2O_4{}^-$, $^{26}CN^-$, and $^{42}CNO^-$ in DEA-containing particles. The shaded areas represent the 75th and 25th percentiles.

985

986

987
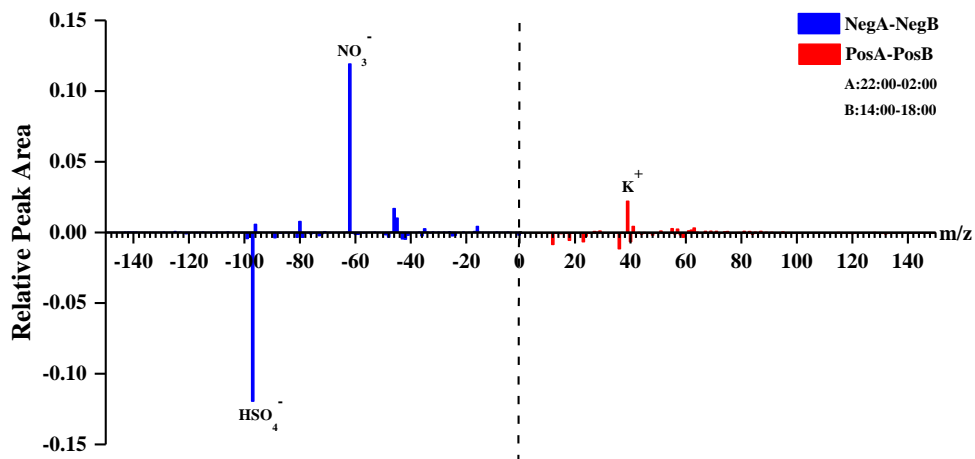
988

Figure 8. Differential mass spectra of DEA-containing particles between 22:00–02:00

and 14:00–18:00.

991

992

993

994

995
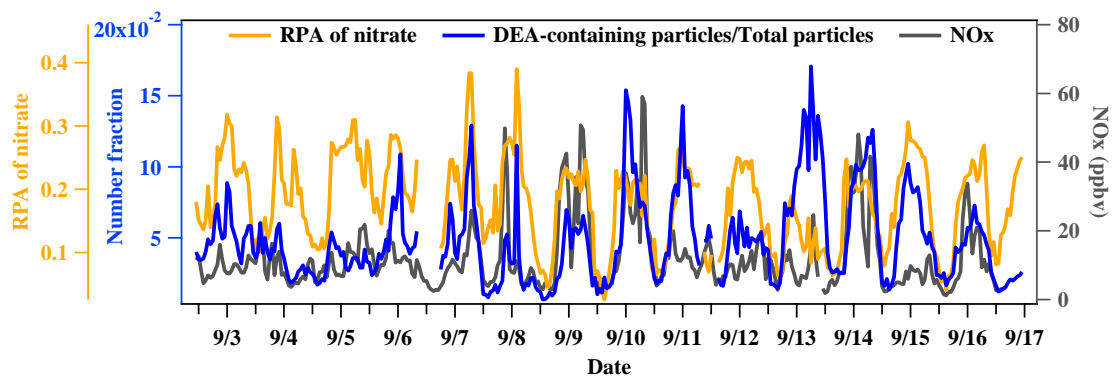
996

Figure 9. Temporal trends of RPA nitrate in DEA-containing particles, number

fraction of DEA-containing particles in total particles, and NOx concentration.

999

1000

1001

1002

1003

1004

Figure 10. Temporal trends of TMA- and DEA-containing particle counts, and number fractions of nitrate, sulfate, and ammonium in TMA- and DEA-containing particles.

1005
1006
1007

1008

1009

1010

Figure 11. Temporal trends of the relative acidity ratios (Ra, Ra$^{'}$) in TMA- and DEA-containing particles.

1011
1012

1013